ESTIMATING LONG-TERM SOLAR IRRADIANCE VARIABILITY: A NEW APPROACH

ANNE VIGOUROUX[1], JUDIT M. PAP[2], PHILIPPE DELACHE[1,*]
[1] *Laboratoire Cassini, associé au C.N.R.S. (U.M.R. 6529), Observatoire de la Côte d'Azur, B.P. 229, F-06304, NICE Cedex 04, France*
[2] *Division of Astronomy and Astrophysics, Department of Physics, University of California, Los Angeles, Los Angeles, CA 90095-1562, U.S.A. and Jet Propulsion Laboratory, California Institute of Technology, MS 169-506, 4800 Oak Grove Dr., Pasadena, CA 91109*

(Received: 5 July 1996; accepted: 5 May 1997)

Abstract. The detection of solar irradiance variations (both bolometric and at various wavelengths) by satellite-based experiments during the last one and a half decades stimulated modeling efforts to help identify their causes and to provide estimates of irradiance data for those time intervals when no satellite observations exist. In this paper we present estimates of the long-term irradiance changes developed with Fourier and wavelet transforms. The month-to-month irradiance variations, after removing the solar cycle related long-term changes, are studied with the cross-correlation technique. Results of the analysis reveal a significant phase shift at 3 months between the full disk magnetic field strength and total solar and UV irradiance, with irradiance leading the magnetic field variability. In addition to this time delay between the changes in solar irradiance and the magnetic field, a 10-month phase shift has been found between the UV flux at 280 nm and total solar irradiance corrected for sunspot darkening. The existence of these phase shifts suggests the possibility of a coupling between the physical processes taking place below, in, and above the photosphere.

1. Introduction

The total radiation received from the Sun on the top of the Earth's atmosphere is called solar constant. Irradiance observations from space over the last 18 years demonstrated that its value changes with time as an effect of the waxing and waning solar activity (e.g., Fröhlich, 1994). Since the total energy flux of the Sun is one of the main natural driving forces of the Earth's atmospheric and climate system, it is essential to understand the observed irradiance changes. One of the main interests is to reconstruct the irradiance changes back to the time of the Maunder Minimum (1645-1705), when only little magnetic activity occurred on the Sun (Ribes and Nesme-Ribes, 1993). One very interesting aspect of this solar anomaly is its concurrence with a cold period in Europe and the Atlantic region, known as the Little Ice Age. It has been shown that changes as little as 0.3% in total irradiance over several decades may have contributed to temperature anomalies observed during the Maunder Minimum (e.g., Lean *et al.*, 1994; Nesme-Ribes, Sokoloff, and Sadourney, 1994). Moreover, current studies indicate that solar radiative forcing has been a more important factor in recent climate change than former estimates would imply (e.g., Reid, 1997).

[*] Deceased on October 13, 1994

The detection of total irradiance variations by satellite-based experiments and their potential role in climate change have stimulated modeling efforts to help identify their causes and to provide estimates of irradiance data for time intervals when no satellite observations exist. Because of the lack of an adequate quantitative physical model of the variations in total irradiance, the current models are developed with linear regression analysis from proxy indicators of solar activity. However, the question is whether these empirical models can reasonably reconstruct and predict the changes in solar irradiance. It has been shown that the regression models of total irradiance underestimate the observed changes during solar maximum (Foukal and Lean, 1988) and the regression coefficients also change as a function of the solar cycle (Pap *et al.*, 1994; Fröhlich, 1994). In addition, the time series of solar irradiance, either space-borne or ground-based surrogates, can be regarded as "pseudo-periodic" signals with variable spectral properties (e.g., change of periods, amplitudes, and phases) (Lean and Repoff, 1987; Fröhlich and Pap, 1989; Bouwer, 1992). The currently used regression models of solar irradiance and its surrogates cannot distinguish between periodic or seasonal components and an error-term describing the essentially random fluctuations of the time series (Priestly, 1993). Therefore, instead of a standard regression model, special methods are required to determine the spectral properties of the investigated time series.

Fröhlich and Pap (1989) have demonstrated that it is very important to study irradiance changes in the frequency domain. Results of multivariate spectral analysis show that considerable variation remains unexplained in both solar total and UV irradiance by the effect of sunspots and faculae and the amplitude of this residual variability changes with the phase of the solar cycle (Pap and Fröhlich, 1992). It is not yet clear whether the unexplained variations are related to additional solar events, such as large scale motions (Ribes, Mein, and Mangeney, 1985), temperature changes (Kuhn, Libbrecht, and Dicke, 1988) and radius changes (Delache, Laclare, and Sadsaoud, 1986; Gavryusev *et al.*, 1994; Ulrich and Bertello, 1995), or whether they are associated with instrumental effects and/or limitation of the previously used analysis techniques.

The main goal of this paper is to study the long-term changes in total irradiance and its surrogates with using Fourier and wavelet techniques. For this purpose, any changes shorter than the solar rotation are filtered from the data by calculating monthly averages in a similar way as published by Pap, Vigouroux, and Delache (1996, hereafter Paper I). The uncertainty of the monthly averages, the so-called dispersion, is calculated from the corresponding daily values, analogous to the calculation of the standard deviation. In Paper I we have shown that the dispersion values change with the phase of the solar cycle, being higher during maximum activity conditions. Using these time-dependent dispersion values as 'error-bars' (thereafter called as 'dispersion-bars'), we invert the Fourier and wavelet transforms to reconstruct the long-term changes in total irradiance and its surrogates. As a next step, the residual time series between the monthly averages and the inverse Fourier/wavelet transforms are examined by means of the cross-correlation technique.

Total solar irradiance, used in this study, was observed by the ACRIM I radiometer on the Solar Maximum Mission (SMM) satellite (Willson and Hudson, 1991) and the Nimbus-7/ERB radiometer (Hoyt *et al.*, 1992). The Photometric Sunspot Index calculated by Fröhlich, Pap, and Hudson (1994), the Mg II h & k core-to-wing ratio (Donnelly, White, and Livingston, 1994), and the full disk magnetic flux (Harvey, 1994) are used as proxy data for solar magnetic activity. Detailed description of these data is provided in Paper I.

2. Study of long-term variations by the wavelet and Fourier techniques

Signal processing is essential for many scientific studies. It allows us to describe the data we have from various sources and to model the variations of greatest interest. But for an optimal description, the reconstructed time series have to reproduce the main features of the original signals. In the case of studying non-stationary signals, when transient events appear which cannot even be predicted on a statistical basis, there is an urgent need to develop and apply techniques different from the Fourier transform. The wavelets are part of these techniques. The wavelet transform can be defined as a time and scale transform and it consists of making successive projections on basis functions which are located in time. Each basis function is a time-dilation of the previous basis (and this corresponds to scale information which could be compared to the information contained in a frequency band). A complete description of the wavelet technique is given by Meyer (1993).

One of our goals is to find an adequate way to represent the long-term variations in total irradiance and its surrogates. As a first step, any changes shorter than the solar rotation were filtered from the data by calculating monthly averages. To establish the uncertainty of these monthly averages, the dispersion of the daily data within 30-days was derived from the corresponding daily values in a similar way as calculating the standard deviations. Although the dispersion values also represent the uncertainties of the measured data, in this analysis they are mainly related to the fluctuations in the data due to the growth, evolution, and decay of active regions on time scales of days to weeks. Because of this, as shown in Paper I, the dispersion values change with the phase of the solar cycle, being higher during maximum activity conditions. Following the method described by Vigouroux and Delache (1993), we first simulated the short-term variations from the dispersions associated with the monthly means. These short-term variations, which are mostly solar in their origin, are unwanted in our derivation of the long-term variations. As a next step, we calculated the threshold level from the Fourier and wavelet transforms of the simulated short-term variations. Data falling below the threshold level were excluded from the analysis. Because of the changing dispersion-bars over the solar cycle, the threshold level is also time-dependent in the wavelet analysis. In this way a relevant model of the long-term variations in the appropriate signal

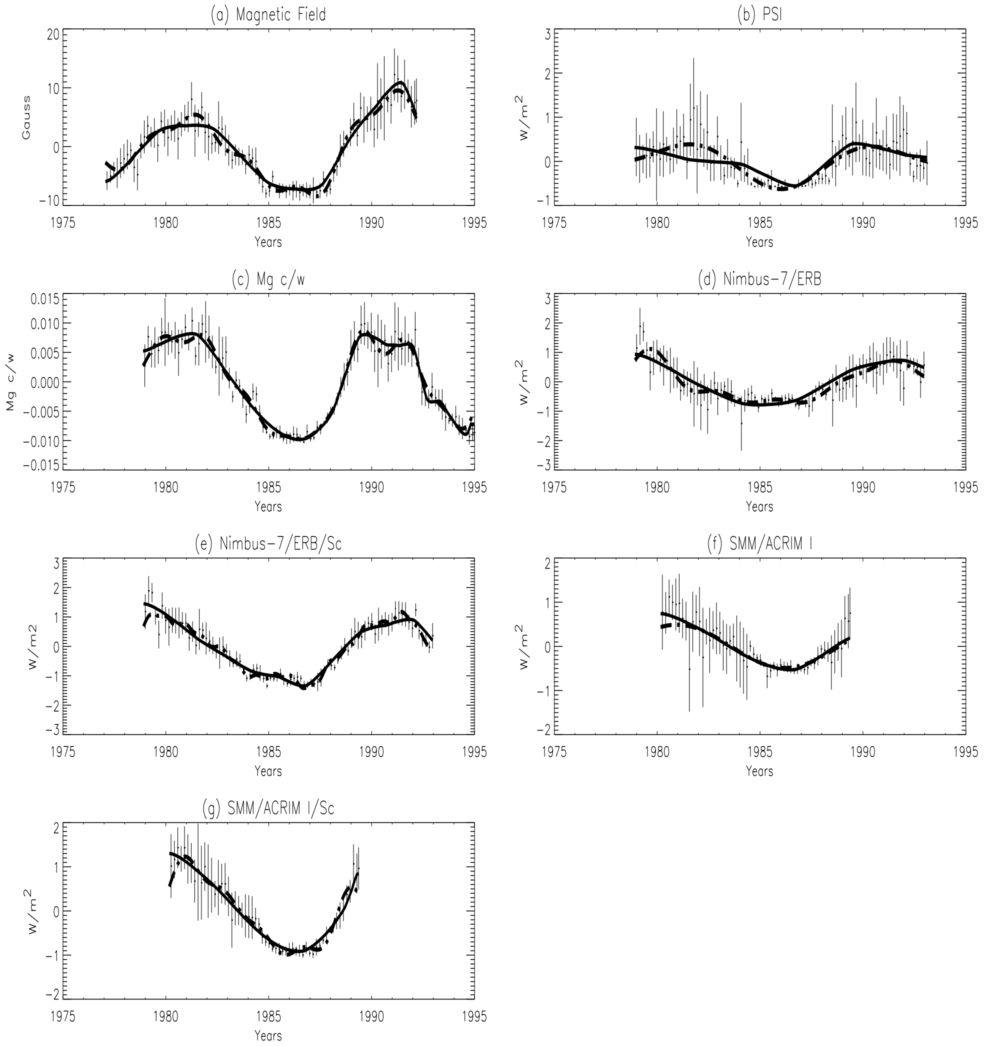

Figure 1. Long-term variations as revealed by the wavelet (heavy solid lines) and Fourier (heavy dot-dashed lines) techniques are presented. The monthly averages of the examined time series are plotted with their respective dispersion-bars. For the visibility of the dispersion-bars, they are shown for every two months.

can be determined, whereas the rest represents the month-to-month variations. In the discussions to follow we compare the results gained by the Fourier and wavelet transforms, respectively.

Figures 1(a-g) represent the monthly averages of the examined time series with their respective dispersion-bars. The full disk magnetic field is shown in Figure 1(a), the Photometric Sunspot Index (PSI) in Figure 1(b), the combined Nimbus-7/NOAA9 Mg core-to-wing ratio (Mg c/w) in Figure 1(c). Figures 1(d) and 1(e)

Table I

Table I contains the inverse Fourier and wavelet transformation characteristics. In Column 1 we list the examined datasets. Column 2 gives the number of data in the various time series. In column 3 we indicate the processing techniques used, FP stands for Fourier Processing, whereas WP means Wavelet Processing. Column 4 provides the percentage of Fourier and wavelet coefficients above the threshold. In column 5, ρ is the cross-correlation coefficient between the 'models' and the original averaged data.

data	number of points	signal processing	nb coefficients (in %)	ρ
Mg c/w	197	FP	8.6	0.99
		WP	9.4	0.99
Mag. Field	185	FP	5.46	0.97
		WP	3.53	0.97
PSI	174	FP	2.34	0.99
		WP	1.17	0.99
Nimbus-7/ERB	172	FP	5.46	0.96
		WP	1.57	0.94
Nimbus-7/ERB/S_c	172	FP	6.25	0.98
		WP	4.31	0.98
SMM/ACRIM I	113	FP	1.56	0.96
		WP	2.36	0.97
SMM/ACRIM I/S_c	113	FP	7.81	0.99
		WP	5.51	0.99

show the Nimbus-7/ERB total irradiance and its corrected value for sunspot darkening (S_c), whereas the same is shown for the SMM/ACRIM I total irradiance in Figures 1(f) and 1(g). The gaps in the data were filled by linear interpolation. The dispersion of the interpolated data points have been taken as the maximum between the dispersion values of the two neighboring points in order to avoid giving too much weight to the interpolated data. As a consequence, in the case of the ACRIM I total irradiance the dispersion values are rather large at the end of 1983 and at the beginning of 1984, when there was a big gap in the data. For both the Fourier and wavelet analyses, 256 points of each time series have been taken. Since the ACRIM I time series covers a much shorter time interval than the rest of the data, the number of the monthly averages treated at once has been reduced to 128 points.

The heavy dot-dashed lines of Figures 1(a-g) show the inverse Fourier transforms, whereas the heavy solid lines represent the corresponding inverse transforms of the wavelet processing. Results gained with both techniques are summarized in

Table I, where the number of original data points in each series is listed. The percentage of the Fourier and wavelet coefficients above the threshold is listed in column 4. To compare the Fourier and wavelet 'models' with the monthly averages of the data, the correlation coefficients between the reconstructed and original data have been calculated as:

$$\rho = \frac{\sum D_i * \bar{D}_i * W_i}{\sqrt{\sum {D_i}^2 * W_i * \sum {\bar{D}_i}^2 * W_i}}$$

where D_i are the monthly averages of the data and $\bar{D}_i$ represent the data reconstructed either with FFT or wavelet. The W_i weighting function is calculated as $W_i = 1/\delta_i^2$ where δ_i are the standard deviations of the monthly data.

As can be seen from Table I, the number of coefficients above the threshold is smaller in the case of the wavelet processing than in the case of the Fourier transform (except for Mg c/w and ACRIM I total irradiance). This corresponds to the sensitivity of wavelets to unequal error bars, represented by the dispersion in our analysis. As can be seen from Figure 1, the dispersion values are much larger during solar maximum, due to the larger day-to-day variability, than during minimum activity (see also Paper I). Therefore, the wavelet transform takes less into account the variability during solar maximum than during solar minimum. In other words, the smaller dispersion bars have much more weight than the larger ones, then, the wavelet will retain more coefficients during solar minimum. In contrast, the Fourier transform is not sensitive at all to the level of the dispersion bars. Since the Fourier transform is a simple superposition of sinusoidal waves not localized in time, it can appear that the large variations in solar irradiance and its surrogates during solar maximum will also appear at the time of solar minimum after the inversion, although they are not present in the real time data. The appearance of these oscillations introduced by the Fourier transform can be recognized in Figures 1(a), 1(d), 1(e) and 1(g).

As can be seen from Figure 1, the maximum of solar cycle 21 occurred in 1981 in the monthly average values of the magnetic field, whereas total solar irradiance already started to decrease in 1979. We also note that the dispersion values, representing the short-term changes within a month, are very similar between late 1978 and 1981. This indicates that the level of solar activity was already high at the beginning of the Nimbus-7/ERB irradiance observations. In addition, the wavelet reconstruction of PSI also shows a slow decrease from 1979. However, it is difficult to clarify whether the early maximum of total irradiance during solar cycle 21 is a real effect (e.g. Willson and Hudson, 1991) or it is related to instrumental drifts at the beginning of the operation of the radiometers (e.g. Foukal and Lean, 1988; Lee *et al.*, 1995).

In addition to the controversy of the time of solar maximum of total irradiance during solar cycle 21, we have no adequate knowledge about the real changes in total irradiance during the maximum of solar cycle 22. As can be seen from

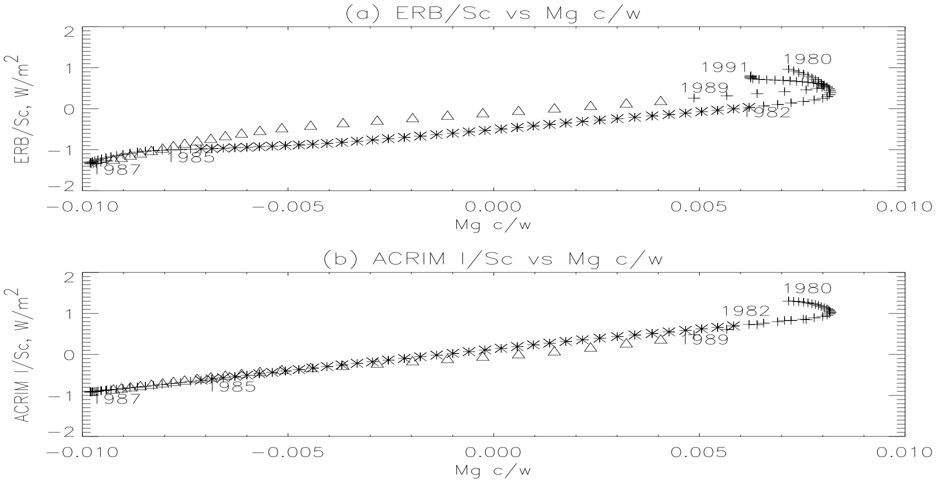

Figure 2. Scatter plot diagram between the Nimbus-7/ERB total irradiance corrected for sunspots darkening and Mg c/w for solar cycles 21 and 22 is plotted on the upper panel and the same is shown for the SMM/ACRIM I data (lower panel). Data for the declining portion of cycle 21 are plotted with asterisks, whereas the triangles represent data for the rising portion of cycle 22. The crosses represent the minimum of solar cycle 21 and the maxima of cycles 21 and 22.

Figure 1, the Nimbus-7/ERB total irradiance and the full disk magnetic field show a similar pattern during the rising portion of solar cycle 22. Namely, both indices reached a small maximum in 1989 and they continued to rise and reached the maximum values in late 1991 (see also Harvey, 1994). In contrast, both PSI and the Mg c/w ratio (and other solar indices which are not presented in this paper) show that the maximum time of cycle 22 already occurred in late 1989 and a secondary maximum took place in 1991. Unfortunately, the SMM/ACRIM I observations were terminated before the primary maximum of solar cycle 22 and the UARS/ACRIM II observations started two years later, in October 1991. An additional set of total solar irradiance is provided by the ERBE program on the NOAA9 and ERBS satellites. Although these observations have been taken only once in every two weeks, the long-term profile of the ERBE data also indicates that the maximum of total solar irradiance occurred in late 1989 (Lee *et al.*, 1995).

To examine the linear association between the changes in total irradiance and its surrogates during solar cycles 21 and 22, we present the scatter plot diagram between the ERB total irradiance corrected for sunspot darkening and the Mg c/w ratio (Figure 2(a)). The same is shown for the ACRIM I values in Figure 2(b). The asterisks indicate the values for the declining portion of solar cycle 21, whereas the triangles show them for the rise of cycle 22. The crosses represent the maxima of cycles 21 and 22 and the minimum of cycle 21. As can be seen, there is a clear hysteresis in the case of the Nimbus-7/ERB data. This indicates that the decrease of the ERB total irradiance corrected for sunspot darkening and the Mg c/w ratio was in phase during the decline of solar cycle 21, but the Mg c/w ratio increased much faster than the ERB total irradiance during the ascending phase of cycle 22. In contrast, this hysteresis is not seen in the case of the ACRIM I irradiance. It is not clear as yet whether the hysteresis in the case of the ERB data is a real effect or it is related to a possible but yet uncorrected instrument degradation caused by the rapid rise in the energetic particles and UV fluxes during the rising portion of cycle 22 and/or to other instrumental effects (Lee *et al.*, 1995). It should be underscored that from climate point of view, the most important task is to estimate correctly the amplitude of the relative changes between the maximum and minimum times of the solar activity cycle.

3. Study of the short-term changes in total irradiance and its surrogates on monthly time scales

In the discussion to follow we compare time series with the same length, namely between January 1, 1980 and March 31, 1992, except for the ACRIM I data which are available only from February 16, 1980 to June 1, 1989. In order to remove the long-term variations over the solar cycle, the appropriate Fourier and wavelet reconstructions have been subtracted from the observed data. The residual time series, representing the month-to-month variability, are plotted in Figures 3(a-g). The dot-dashed lines show the residuals after removing the Fourier reconstructions, whereas the solid lines represent the residuals after removing the long-term trend by means of the wavelet reconstructions. As can be seen from Figure 3, there is no significant difference between the Fourier and wavelet residuals during high solar activity conditions. In contrast, the difference between the Fourier and wavelet residuals is more pronounced for solar minimum. As can be seen, there are peaks in the various datasets during the declining portion of cycle 21 with decreasing amplitudes toward solar minimum, and the larger monthly variability returns during the rise of cycle 22.

3.1. Power Spectral Density of the residuals

In order to further examine the month-to-month variability in various datasets, the power spectral densities (PSD) have been calculated and shown in Figures 4(a-g). The PSD values represent the power spectra estimated by means of the Fourier transform of the auto-correlation of the residuals weighted with a Hanning window. In this way one can avoid giving too much weight to data points which are far from the center of the auto-correlation. The dot-dashed lines represent the PSD of the Fourier residuals and the solid lines show the PSD of the wavelet residuals. Except for the periodicities longer than 20 months, the PSDs are almost the same for both the Fourier and wavelet residuals. The periodicities longer than 20 months are more pronounced in the wavelet residuals than in the Fourier ones.

In the case of total irradiance measured by the Nimbus-7/ERB radiometer there are two periodicities with high amplitudes at 85.3 and 32 months. In the case of

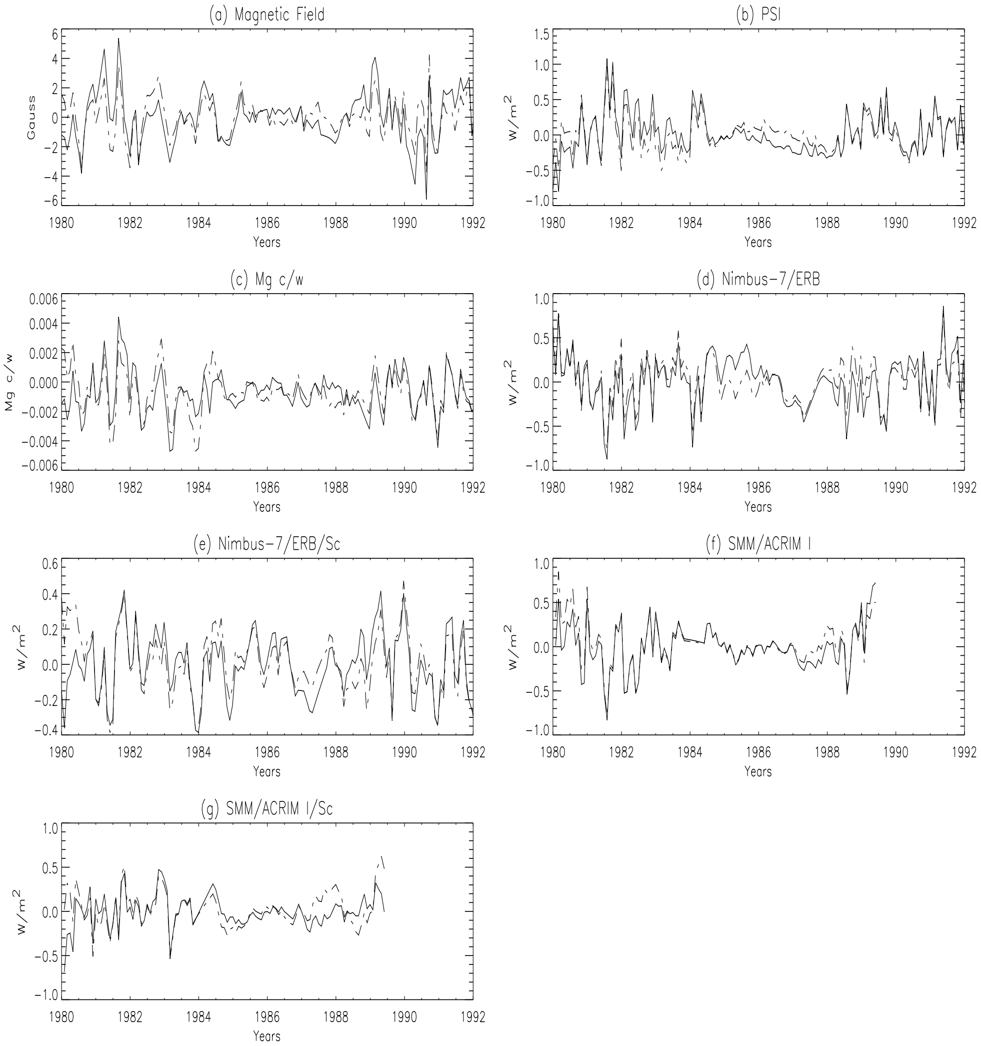

Figure 3. The wavelet (solid lines) and Fourier (dot-dashed lines) residuals of the time-series are plotted after removing the long-term trends.

PSI the main periods are found at 85.3 and 42.7 months. This latter periodicity is also found in ACRIM I total irradiance (together with a period at 51.2 months). Note that the 32 months periodicity is also present in the full disk magnetic flux and it is about 28.5 months in Mg c/w. We note here that a periodicity around 30 months has also been found in the solar diameter (Delache, Laclare and Sadsaoud, 1985 and Gavryusev *et al.*, 1994) as well as in the neutrino flux (Gavryusev and Gavryuseva, 1994) with a high confidence level. Wolff and Hickey (1987) have proposed that a periodicity around 30 months could be found in global, long-

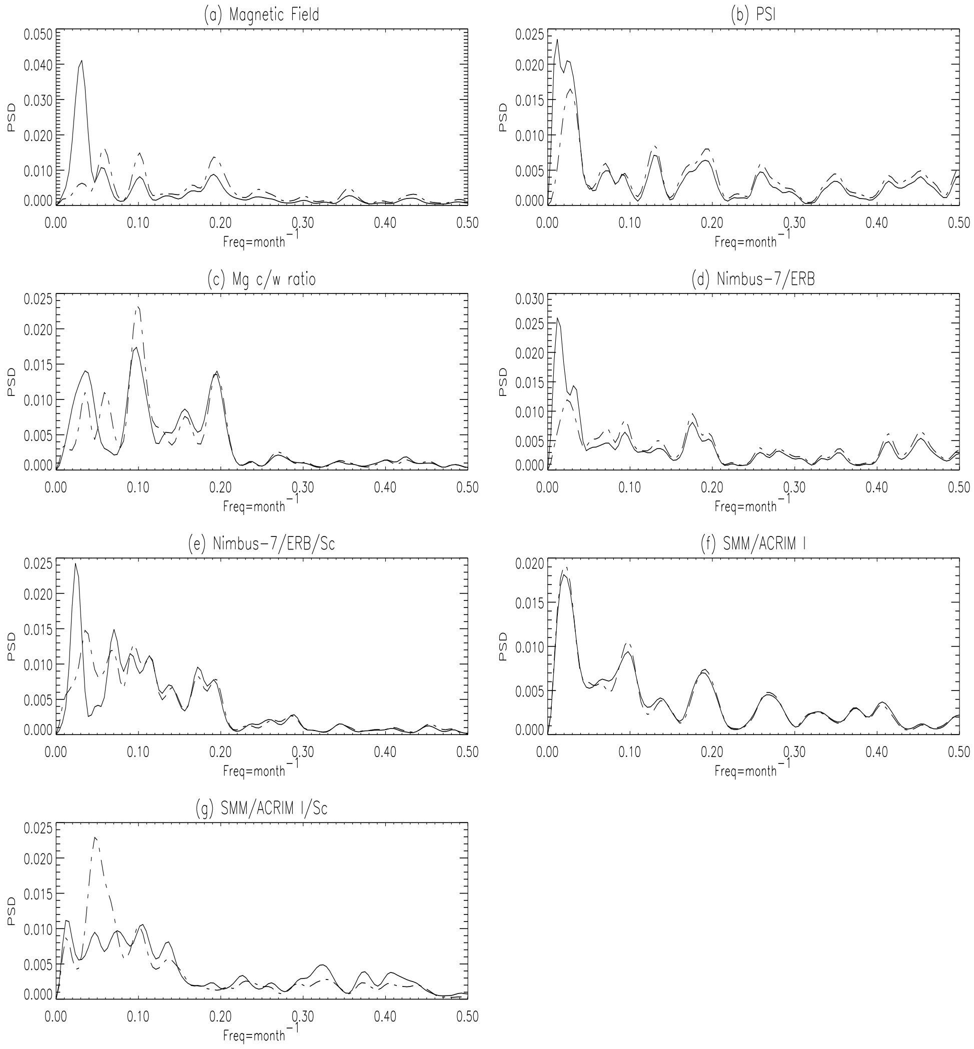

Figure 4. Power Spectral Densities (PSD) of the wavelet (solid lines) and Fourier (dot-dashed lines) residuals of the examined time-series are presented.

period solar oscillations caused by interferences of internal gravity modes.

In the case of the ERB total solar irradiance corrected for sunspot darkening, the wavelet residuals show a large peak again at 32 months (Figure 4(e)). It is interesting to note that the PSDs of the ACRIM I and ERB total irradiances corrected for sunspot darkening are quite different. The Fourier residuals show a big peak, in fact the most significant one, in the ACRIM I/S_c data around 20 months period which is completely missing in the ERB/S_c data. The wavelet residuals of the ERB/S_c signal reveal the most significant period around 42 months.

Table II
Results of cross-correlation between PSI and irradiance indices are summarized. Column 1 refers to the corresponding Figure. Column 2 shows the times series used in the cross-correlation analysis. Columns 3 and 4 give the time lag in months at which the main peak has been found and the cross-correlation coefficients, respectively. Columns 5 and 6 provide the same as Columns 3 and 4 for the significant secondary peak(s), if there is any.

Ref. of the figure	cross-corr. between	main peak at	main peak value	secondary peaks at	secondary peaks value
5a	ERB–ACRIM I	0	0.6	-	-
5b	ERB/S_c–ACRIM I/S_c	0	0.52	-	-
5c	PSI–ERB	0	-0.58	13	0.25
	–			18	0.26
5d	PSI–ACRIM I	0	-0.38	2	0.29

This period is missing in the ACRIM I/S_c but two smaller peaks are seen around 85 and 21 months. Part of the discrepancies between the ERB and ACRIM I total irradiance corrected for sunspot darkening may result from the different length of the time series, especially from the fact that the Nimbus data and the used solar activity indices cover the maximum of solar cycle 22 as well.

It is interesting to note that the PSD of all the examined time series show some energy around 5 and 10 months periodicities. These periodicities have been shown in various solar events, such as flares, proton events, the CaK plage index, 10.7 cm radio flux, and solar radius, (Rieger et al., 1984; Bai and Sturrock, 1991; Pap, Tobiska and Bouwer, 1990; Gavryusev *et al.*, 1994), but their origin is not yet well understood. Pap, Tobiska and Bouwer (1990) have suggested that the periodicity around 5 months or 150 days may be related to complexes of activity, in which new activity appears from time to time. On the other hand, Bai and Sturrock (1991; 1993) consider the 154-day periodicity as one of the subharmonics of a fundamental period of 25.8 days.

3.2. Cross-correlation between the residual time series

To further study the linear association between the month-to-month changes in various datasets, we have performed a cross-correlation analysis. Since the wavelet transforms follow closer the original signals, we have analyzed in detail only the wavelet residuals of total irradiance and its surrogates after removing the long-term trends. The horizontal dashed lines (in Figures 5-8) represent the significance level of the cross-correlation coefficients. It has been shown that for a random time series, which has the same number of data as the residuals, 95% of the values of the cross-correlation lie between $\pm 2/\sqrt{N}$, where $N = 149$ (Chatfield, 1984).

Table III
Results of cross-correlation between the Mg c/w and irradiance indices are summarized. The description of each column is the same as given in the caption of Table II.

Ref. of the figure	cross-corr. between	main peak at	main peak value	secondary peaks at	secondary peaks value
6a	Mg c/w–PSI	1	0.42	6	0.19
6b	Mg c/w–ERB	1	0.24	11	0.2
	–			-9	0.2
	–			21	0.12
	–			-20	0.21
6c	Mg c/w–ERB/S_c	0	0.58	11	0.26
6d	Mg c/w–ACRIM I/S_c	1	0.32	10	0.2

Table IV
Results of cross-correlation between the magnetic field strength and irradiance indices are summarized. The description of each column is the same as given in the caption of Table II.

Ref. of the figure	cross-corr. between	main peak at	main peak value	secondary peaks at	secondary peaks value
7a	mag. field–ERB	0	-0.2	-9	0.33
7b	mag. field–ACRIM I	-1	-0.14	-9	-0.22
7c	mag. field–ERB/S_c	0	0.38	6	0.2
	–			11	0.25
	–			-3	-0.23
7d	mag. field–ACRIM I/S_c	1	0.4	-	-
7e	mag. field–Mg c/w	0	0.5	6	0.28
	–			11	0.25
	–			-3	-0.32
7f	mag. field–PSI	0	0.51	5	0.3
	–			9	0.15

Positive lags indicate that the first time series, as shown in the main title of the appropriate plots, is leading the second one. Summary of the main characteristics of the results of the cross-correlation (Figures 5-8) are presented in Tables II-IV.

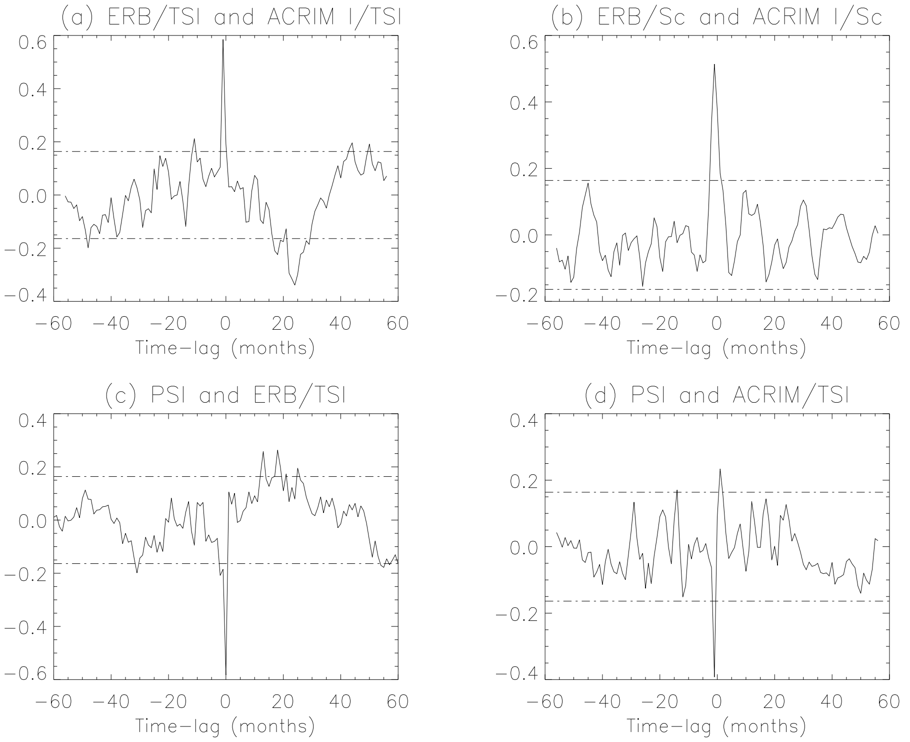

Figure 5. Results of the cross-correlation between: the wavelet residuals of the Nimbus-7/ERB and SMM/ACRIM I total irradiance (a) as well as their corrected values for sunspot darkening (b), the PSI residual time-series and the wavelet residuals of the Nimbus-7/ERB (c) and SMM/ACRIM I (d). The horizontal dashed lines give the significance level of the cross-correlation coefficients.

3.2.1. Cross-correlation between Total Irradiance and PSI

The cross-correlation between the Nimbus-7/ERB and SMM/ACRIM I total irradiances as well as between their values corrected for sunspot darkening are presented in Figures 5(a) and 5(b), respectively. As can be seen, the maximum correlation occurs at zero time lag in both cases, however the correlation is rather low (see Table II). Note that the correlation has been calculated between the ERB and ACRIM I total irradiances as a function of time as well (not shown here). It has been found that there is a reasonably good correlation during the years of high solar activity. The correlation between the ERB and ACRIM I data decreases significantly during the time interval of the spin operational mode of the SMM satellite. The lowest correlation is found at the time of solar minimum when the ERB data show considerably larger variations than the ACRIM I data (see also Fröhlich, 1994).

Figures 5(c) and 5(d) (see also Table II) show the results of the cross-correlation between the residuals of the PSI function and both Nimbus-7/ERB (Figure 5(c))

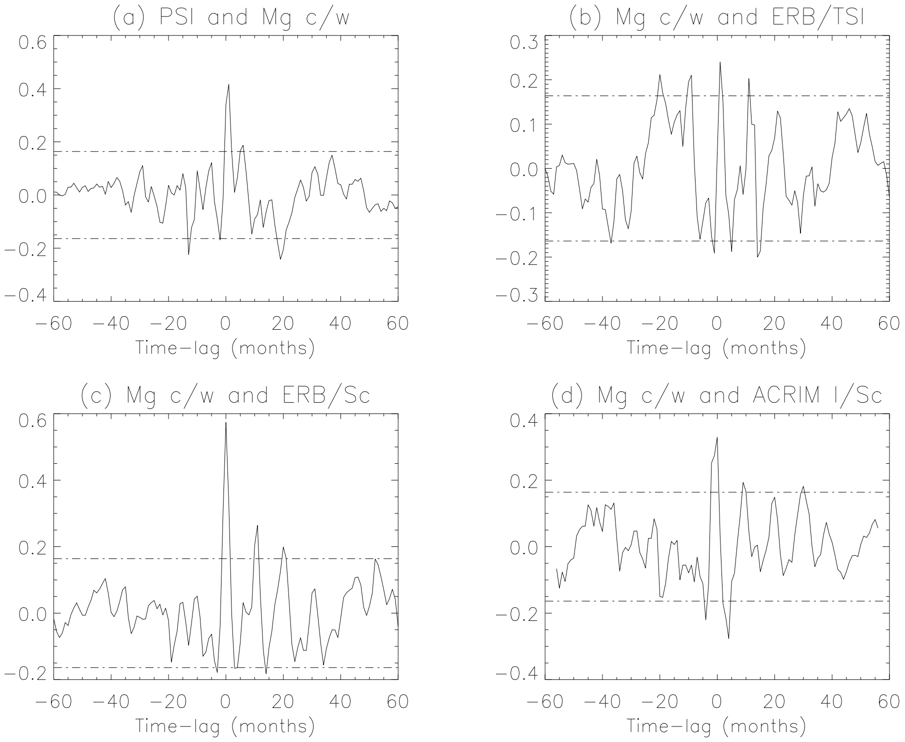

Figure 6. Cross-correlation between: the PSI and Mg c/w wavelet residual time-series (a) and Mg c/w and the Nimbus-7/ERB total solar irradiance wavelet residual time-series (b), the Mg c/w and ERB/S_c (c), Mg c/w and ACRIM I/S_c) wavelet residual time-series (d) are presented in Figure 6(d). The horizontal dashed lines give the significance level of the cross-correlation coefficients.

and SMM/ACRIM I (Figure 5(d)) total solar irradiance. As can be seen, the two cross-correlations are quite different. There is a negative correlation at zero time lag in both cases, indicating that sunspots reduce total irradiance.

3.2.2. Cross-correlation between Total Irradiance and the Mg c/w ratio

The results of the cross-correlation between PSI and the Mg c/w ratio are presented in Figure 6(a). In this case the maximum correlation was found at 1 month time lag (see Table III), indicating that PSI is leading the Mg c/w. Note that Donnelly *et al.* (1983) have also reported that peaks in solar indices related to strong magnetic fields of sunspots occur about a month prior to enhancements in the Mg c/w ratio. This 1 month time lag has been attributed to the evolution of active regions. Namely, at the beginning of the formation of active regions, the effect of sunspots are dominant and dips occur in total irradiance. As the active regions evolve and age, the plages spread over large areas causing peaks in both Mg c/w and total solar irradiance.

The cross-correlation between the Mg c/w ratio and the ERB total irradiance is shown in Figure 6(b). The maximum of the cross-correlation occurs at 1 month time lag with total irradiance leading Mg c/w. But, when the effect of sunspots is removed from total irradiance (see Figures 6(c) and 6(d)), the maximum of the cross-correlation is found for 0 lag, with a high value of the correlation. Note that the peak representing the maximum correlation between the Mg c/w ratio and ACRIM+PSI is wider than for ERB and the correlation is also somewhat lower. The secondary peaks seen in Figure 6 (see also Table III) for time lag around ± 10 months may be due to the corresponding periodicity detected in the PSD of the investigated time-series (see Figure 4) but see section 3.2.4 for further discussion.

3.2.3. Cross-correlation between Solar Irradiance and the Magnetic Field Strength
Since solar irradiance variations are primarily driven by the magnetic activity, we have also compared the wavelet residuals of the full disk magnetic field values with the residuals of total and UV irradiance, the latter one represented by the Mg c/w. The results of the cross-correlation between the magnetic field and the ERB and ACRIM I total irradiance are presented in Figures 7(a) and 7(b), respectively.

As can be seen, there is a slight anti-correlation (see Table IV) between the magnetic field and total irradiance at zero and -1 month time lags with total irradiance leading magnetic field. Although the magnetic field is the strongest in sunspots, its value is also enhanced in the presence of bright magnetic features which increase total irradiance. Therefore, the anti-correlation between the magnetic field and irradiance deficits due to sunspots is less visible than in the case of the cross-correlation between total irradiance and PSI (Figure 5(c) and 5(d)). We note that this anti-correlation is less obvious from the ACRIM I data, which covers only the maximum of solar cycle 21. In contrast, the Nimbus-7/ERB operation includes also the maximum time of cycle 22, increasing the number of irradiance events. It is interesting to note that a significant positive correlation has been found around -10 months lag (with total irradiance leading magnetic field) in both cross-correlation results (see Figures 7(a) and 7(b)), which seems to be associated with the sunspot-related irradiance dips and the peaks in the magnetic field.

The cross-correlation between the magnetic field and S_c is presented in Figure 7(c) (ERB/S_c) and Figure 7(d) (ACRIM I/S_c). The same is plotted for the Mg c/w in Figure 7(e). The magnetic field and PSI are directly compared, the results of their cross-correlation are presented in Figure 7(f). As can be seen from Figures 7(c) and 7(e), the results of the cross-correlation are rather similar for the ERB/S_c and Mg c/w, when positive correlations are found at 0-1, 5, and 10 months time lags (for those positive lags, magnetic field is leading total irradiance and Mg c/w) . In the case of the ACRIM I/S_c data (Figure 7(d)), the only significant correlation coefficient is seen at 1 month lag. In the case of the ERB/S_c as well as Mg c/w, there is a negative correlation at -3 months time lag, indicating that Mg c/w and total irradiance lead magnetic field. This -3 months time lag may be associated with the 5-6 months periodicities found in each dataset, as can be seen in Figure 4.

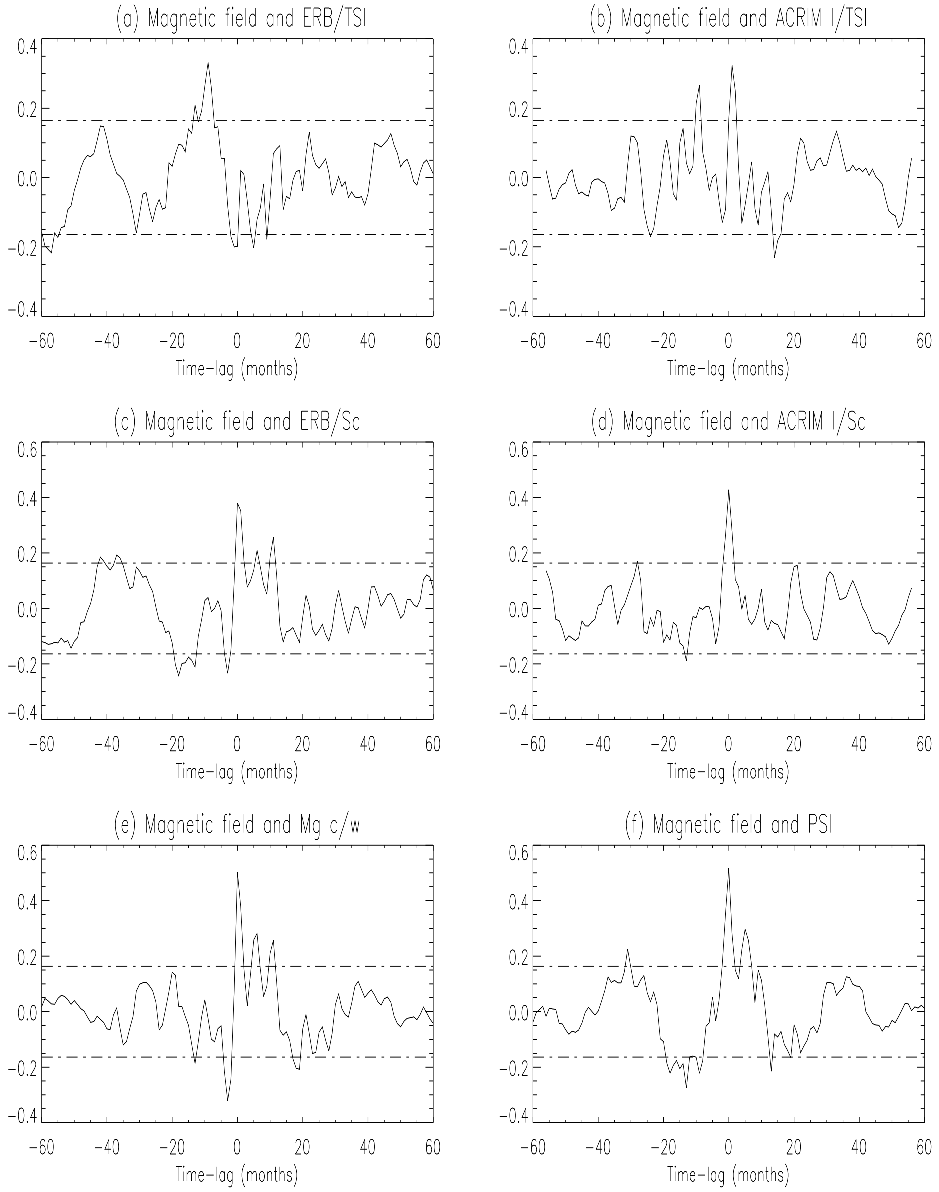

Figure 7. Cross-correlation between the magnetic field and: Nimbus-7/ERB (a) as well as the SMM/ACRIM I (b) total irradiance wavelet residuals, ERB total irradiance corrected for sunspot darkening (c), ACRIM I total irradiance corrected for sunspot darkening (d), the Mg c/w ratio (e), and PSI (f). The horizontal dashed lines give the significance level of the cross-correlation coefficients.

The positive correlation at zero and 1 month time lags indicate that the magnetic fields of plages and the network increase both total and UV irradiances represented by the Mg c/w ratio. The cross-correlation between the magnetic field and the PSI (Figure 7(f)) shows correlation for time lags of 0 and 5 months and a weaker peak at time lag of 10 months (with magnetic field leading PSI).

3.2.4. Cross-correlation between Individuals Scales of the Wavelet Transforms of the Examined Time Series

To further study some of the time delays found between the time series, the cross-correlation has also been calculated between the individual scales of the wavelet transforms of the various residuals corresponding to different frequency bands. The solid lines in Figures 8(a) and 8(b) show the results of the cross-correlation calculated between the wavelet transform of the residuals of the magnetic field and Mg c/w for scale 2 (periodicities between 4 and 8 months) and scale 3 (periodicities between 8 and 16 months), respectively. Figure 8(c) shows the results of the cross-correlation between the magnetic field and Mg c/w for scale 5 (periodicities between 32 and 64 months) of the wavelet transforms. The cross-correlation between the ERB/S_c and Mg c/w for scale 2 and scale 3 is shown in Figures 8(d) and 8(e), respectively. To better understand the results of the cross-correlation, the auto-correlation of the magnetic field and the ERB total solar irradiance corrected for sunspot darkening have also been calculated. The dot-dashed lines of Figures 8(a-c) represent the auto-correlation for the magnetic field, while the results of the auto-correlation of the ERB/S_c are plotted in Figures 8(d) and 8(e). The horizontal line in each panel of Figure 8 shows the 95% significance level of the cross-correlation.

As can be seen from Figure 8(a), the short-term variations (between 4 and 8 months) in the magnetic field and Mg c/w are almost identical. The correlation at zero time lag is 0.74. Furthermore, there is a strong phase coherence for the 5 months periodicity. In contrast, on longer time scales, between 8 and 64 months (Figures 8(b) and 8(c)) the variations in the magnetic field and Mg c/w are quite different. As Figure 8(b) demonstrates, there is a strong negative correlation (r = -0.6) at -4 months time lag, whereas slight positive correlations are seen at time lags of 1-2, +10, and -10, -20, and -30 months. In the case of the 5th scale of the wavelet transform, the only peak is seen at +5 months time lag with r = 0.6. Positive lags for those figures mean that the magnetic field leads Mg c/w. One can note that the shift between auto and cross-correlation becomes bigger with the increasing scale. Although we do not understand the mechanism behind it we note that the same behavior could be obtained with two signals for which the relative phase is a function of frequency.

As can be seen from Figure 8(d), the changes in the ERB total irradiance corrected for sunspot darkening and Mg c/w are almost identical for time scales of 4 to 8 months (wavelet scale 2), but there is a slight correlation for -10 months delay between them. This correlation is better seen on the plot of the cross-correlation

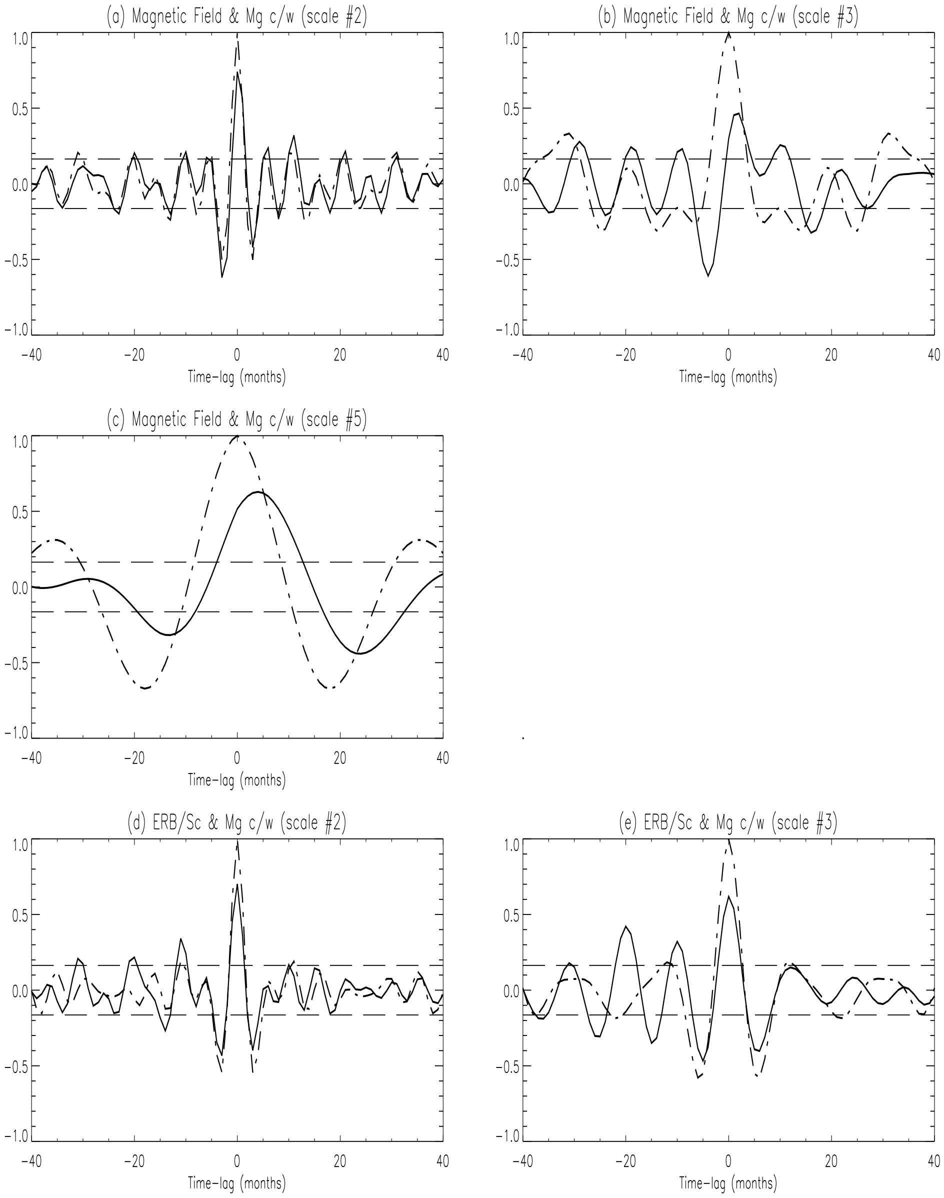

Figure 8. Cross-correlation between the wavelet transform of the wavelet residuals of the magnetic field and Mg c/w: for scale 2 (periodicities between 4 and 8 months; (a)), for scale 3 (periodicities between 8 and 16 months, (b)), for scale 5 (periodicities between 32 and 64 months, (c)). Panels d and e show the cross-correlation between scale 2 and between scale 3 of the wavelet transform of the wavelet residuals of the Nimbus-7/ERB total irradiance corrected for sunspot darkening and Mg c/w, respectively. The horizontal dashed lines give the significance level of the cross-correlation coefficients. Dot-dashed lines in panels (a), (b), and (c) show the auto-correlation of the magnetic field for scales 2, 3, and 5, respectively, while panels (d) and (e) give the auto-correlation of the ERB/S_c total solar irradiance for scales 2 and 3, respectively.

at scale 3 (Figure 8(e)) indicating that Mg c/w is leading total irradiance. We note that this -10 months time delay mostly appears during solar cycle 21, when a 10 months periodicity in the Mg c/w ratio was more visible than during cycle 22. Furthermore, the phase coherence for the 5 months periodicity is not so strong in Fig. 8d than in Fig. 8a.

4. Discussions and Conclusions

The linear association between the variations observed in total solar irradiance, PSI, Mg II h & k core-to-wing ratio, and full disk magnetic field flux has been examined in this paper. Since we are especially interested in studying long-term irradiance changes, the day-to-day variability has been removed from the data by creating monthly averages. The uncertainty of the monthly averages is represented by the dispersion values, which are associated with both measuring uncertainties and short-term variations related to the growth, evolution, and decay of active regions. Using these dispersion values as error-bars, we have reconstructed long-term irradiance changes after filtering the short-term changes. Our results show that the wavelet technique provides a powerful method to estimating long-term irradiance changes since it is well-suited for quasi-periodic data with changing uncertainties and phase shifts occurring every several months. While the Fourier transform cannot distinguish between the unequal dispersion-bars, the wavelet processing is capable of accounting for the smaller dispersion bars, which have been derived for the time interval of solar minimum. In contrast, during solar maximum the dispersion bars in the data are much higher due to the strong day-to-day variability (Pap, Vigouroux, and Delache, 1996).

The short-term changes on monthly time scales in total irradiance and its surrogates have been studied with cross-correlation techniques, after subtracting the long-term Fourier and wavelet reconstructions from the data. Prominent periodicities at 5 and 10 months have been recognized in each dataset. The 5-month (about 154-day) periodicity has recently been attributed to long-lived flow patterns (Sturrock, 1996). The physical origin of the 10-month variability is not yet understood. Significant delays have been found in the cross-correlation of total irradiance and the other solar indices at time-lags of 1, 3, 5, 10, and 20 months. The cross-correlation between solar irradiance and magnetic field is very similar to the autocorrelation of the data on time scales less than 8 months, but the time delays on time scales of 10 months become evident when we study higher scales of the wavelet transforms (corresponding to time intervals larger than 8 months). It has also been shown that there is a 10 month long phase shift between the changes in total irradiance corrected for sunspot darkening and the Mg c/w ratio, used as a proxy for bright magnetic features, the latter leading the former.

The observed time delays between various datasets representing photospheric and chromospheric conditions indicate that the response of the chromospheric layers to the magnetic field variations is quite different than that of the photosphere.

Therefore, using chromospheric indices to estimate the effect of photospheric faculae on total irradiance, especially on long time scales, is not adequate. In order to understand the observed phase shifts between photospheric and chromospheric data, detailed studies of spatially resolved data covering long time intervals are needed. Analysis of high resolution solar images has been in progress in various observatories, such as the National Solar Observatories at Sacramento Peak and Kitt Peak, Big Bear, High Altitude and Mt. Wilson Solar Observatories. The observations of the Michelson Doppler Imager on the SOlar Helioseismology Observatory (SOHO) satellite will dramatically improve our knowledge and capability of interpreting the results described in this paper. One must emphasize that analysis and interpretation of the time-delays found between the magnetic field and solar radiation emitted from different layers of the solar atmosphere will lead to a better understanding of the dynamics taking place below, in, and above the photosphere and will lead to a better understanding of the basic mechanism governing solar variability.

Acknowledgements

The research described in this paper was carried out by the Laboratoire Cassini associé au C.N.R.S. (U.M.R. 6529) of the Observatoire de la Côte d'Azur, University of California, Los Angeles and the Jet Propulsion Laboratory, California Institute of Technology under a contract with the National Aeronautics and Space Administration. The SMM/ACRIM I data used in this study have been produced by the Solar Irradiance Monitoring Group at JPL. The Nimbus-7/ERB data were kindly provided by Dr. D. Hoyt. We acknowledge the NASA/GSFC Ozone Processing Team (OPT) for the Nimbus-7/SBUV1 data and the NOAA/NESDIS for the SBUV2 data. The NSO/Kitt Peak magnetic data used here are produced cooperatively by NSF/NOAO, NASA/GSFC and NOAA/SEL. We are grateful to Dr. Claus Fröhlich and Dr. Eric Fossat for their comments.

References

Bai, T. and Sturrock, P.A.: 1991, *Nature* **350**, 141.
Bai, T. and Sturrock, P.A.: 1993, *Astrophys. J.* **409**, 476.
Bouwer, S.D.: 1992, *Solar Phys.* **142**, 365.
Chatfield, C.: 1984, *The Analysis of Time Series*, Chapman and Hall, New-York, p. 25.
Delache, Ph., Laclare F., and Sadsaoud, H.: 1985 *Nature* **317**, 416.
Delache, Ph., Laclare F., and Sadsaoud, H.: 1986, in J. Christensen-Dalsgaard and S. Frandsen (eds.), *Advance in Helio- and Asteroseismology*, IAU press, p. 223.
Donnelly, R.F., Heath, D.F., Lean, J., and Rottman, G.J.: 1983, *J. Geophys. Res.* **88**, 9883.
Donnelly, R.F., White, O.R., and Livingston, W.C.: 1994, *Solar Phys.* **152**, 69.
Foukal, P. and Lean, J.: 1988, *Astrophys. J.* **328**, 347.
Fröhlich, C. and Pap, J.: 1989, *Astron. Astrophys.* **220**, 272.
Fröhlich, C., Pap, J., and Hudson, H.S.: 1994, *Solar Phys.* **152**, 111.
Fröhlich, C.: 1994, in J. Pap, C. Fröhlich, H.S. Hudson and S.K. Solanki (eds.), *The Sun as a Variable Star: Solar and Stellar Irradiance Variations*, Cambridge Univ. Press, p. 28.

Gavryusev, V., Gavryuseva, E., Delache, Ph., and Laclare, F.: 1994, *Astron. Astrophys.* **286**, 305.
Gavryusev, V. and Gavryuseva, E.: 1994, *Astron. Astrophys.* **283**, 978.
Harvey, K.: 1994, in J.M. Pap, C. Fröhlich, H.S. Hudson and S.K. Solanki (eds.), *The Sun as a Variable Star: Solar and Stellar Irradiance Variations*, Cambridge Univ. Press, p. 217.
Hoyt, D.V., Kyle, H.L., Hickey, J.R., and Maschhoff, R.H.: 1992, *J. Geophys. Res.* **97**, 51.
Kuhn, J., Libbrecht, K.G., and Dicke, R.: 1988, *Science* **242**, 908.
Lean, J. and Repoff, T.P.: 1987, *J. Geophys. Res.* **92 D5**, 5555.
Lean, J., Skumanich, A., White, O.R., and Rind, D.: 1994, in J.M. Pap, C. Fröhlich, H.S. Hudson and S.K. Solanki (eds.), *The Sun as a Variable Star: Solar and Stellar Irradiance Variations*, Cambridge Univ. Press, p. 236.
Lee III, R.B., Gibson, M.A., Wilson, R.S., and Thomas, S.: 1995, *J. Geophys. Res.* **100**, 1667.
Meyer, Y.: 1993, *Wavelets, algorithms and applications*, SIAM (eds.), Philadelphia.
Nesme-Ribes, E., Sokoloff, D., and Sadourney, R.: 1994, in J.M. Pap, C. Fröhlich, H.S. Hudson and S.K. Solanki (eds.), *The Sun as a Variable Star: Solar and Stellar Irradiance Variations*, Cambridge Univ. Press, p. 244.
Pap, J., Tobiska, W.K., and Bouwer, S.D.: 1990, *Solar Phys.* **129**, 165.
Pap, J. and Fröhlich, C.: 1992, in R.F. Donnelly (eds.), *Proc. Solar Electromagnetic Radiation Study for Solar Cycle 22*, SEL, NOAA/ERL, Boulder, p. 62.
Pap, J., Willson, R.C., Fröhlich, C., Donnelly, R.F., and Puga, L.: 1994, *Solar Phys.* **152**, 13.
Pap, J., Vigouroux, A., and Delache, Ph.: 1996, *Solar Phys.*, **167**, 125.
Priestly, M.B.: 1993, paper presented at the International Conference on Applications of Time Series Analysis in Astronomy and Meteorology, Padova, Italy, Sept. 1993.
Reid, G.: 1997, *Climate Change*, in press.
Ribes, J.C. and Nesme-Ribes, E.: 1993, *Astron. Astrophys.* **276**, 549.
Ribes, E., Mein, P., and Mangeney, A.: 1985, *Nature* **318**, 170.
Rieger, E., Kanbach, G., Reppin, C., Share, G.H., Forrest, D.J., and Chupp, E.L.: 1984, *Nature* **312**, 623.
Sturrock, P.: 1996, in K.S. Balasubramaniam, S.L. Keil, and R.N. Smartt (eds.), *Solar Drivers of Interplanetary and Terrestrial Disturbances*, Astronomical Society of the Pacific, Conference Series Vol. 95, p. 42.
Ulrich, R. and Bertello, L.: 1995, *Nature* **377**, 214.
Vigouroux, A. and Delache, Ph.: 1993, *Astron. Astrophys.* **278**, 607.
Willson, R.C. and Hudson, H.S.: 1991, *Nature* **351**, 42.
Wolff, C.L. and Hickey, J.R.: 1987, *Sciences* **235**, 1631.